Diurnal Variation of Simulated Cumulus Convection in Radiative-Convective Equilibrium

Tomoro Yanase and Tetsuya Takemi
Disaster Prevention Research Institute, Kyoto University, Uji, Japan

Abstract

This study investigates the representation of the diurnal variation of cumulus convection in radiative-convective equilibrium states in an area of 200 km by 200 km without large-scale forcing by using a non-hydrostatic model with sub-kilometer horizontal resolutions. The experiment with the horizontal resolution of 200 m successfully reproduced the diurnal variability of the trimodal characteristics of cumulus convection. We demonstrated that the horizontal resolution dependence largely affects the trimodal structure of clouds and the characteristics of precipitation and its diurnal variation. With the coarse resolution of 1600 m, a signature of convective aggregation appeared and the diurnal variation of convection was not clearly seen. We further examined the mechanisms for the diurnal variation of cumulus convection by focusing on the temporal and vertical variations of radiative and latent heating anomalies. The diurnal variability of the static stability caused by both radiative and latent heating plays a role in characterizing the diurnal variation of the cumulus convection.

(**Citation**: Yanase, T., and T. Takemi, 2018: Diurnal variation of simulated cumulus convection in radiative-convective equilibrium. *SOLA*, **14**, 116−120, doi:10.2151/sola.2018-020.)

1. Introduction

Tropical oceanic cumulus convection is known to be organized at various temporal and spatial scales, from individual convection cells, squall lines, cloud clusters, tropical cyclones, to Madden-Julian Oscillation. These phenomena interact with, through their circulation and energy transport, the environments not only at a mesoscale but also on a global scale.

Several studies investigated tropical oceanic convection and its organization by conducting numerical experiments in idealized radiative-convective equilibrium (RCE) states using two or three-dimensional cloud-resolving models (Nakajima and Matsuno 1988; Held et al. 1993; Tompkins and Craig 1998; Robe and Emanuel 2001; Tompkins 2001). Furthermore, some investigated a phenomenon called self-aggregation, in which convective clouds organize as a larger-scale single cluster surrounded by a drier area that suppresses cloud development. As reviewed by Wing et al. (2017), researchers have been discussing what physical mechanisms cause self-aggregation (Wing and Emanuel 2014), how self-aggregation depends on model configuration such as the horizontal resolution and domain size (Muller and Held 2012), and to what extent the simulated self-aggregation is related to the real convective organization (Tobin et al. 2012).

In contrast, there are less studies for the temporal evolution, in particular, diurnal variation than for the spatial structure of convection and its organization (Posselt et al. 2008; Yang 2018; Jeevanjee and Romps 2013). It is probably because studies paid attention mostly to a quasi-stationary climate state after long time integration over several weeks or months in RCE. Accordingly, most RCE studies have used idealized shortwave radiation that does not change with time. On the other hand, if a high spatial-resolution is employed in numerical experiments, the integration time period is limited (Khairoutdinov et al. 2009). Few studies have investigated the influences of diurnal variation on convective activities in RCE. Although Yashiro et al. (2016) investigated a resolution dependence of the diurnal cycle of precipitation in a global cloud-resolving simulation, it is not clear how fine horizontal resolution is required to represent a diurnal variation of convective activities in RCE using a regional cloud-resolving model.

In this study, we conducted numerical experiments of the diurnal variation of cumulus convection in RCE states in which temporal variation of shortwave radiation is taken into account. Here, we aim to elucidate mechanisms for the organization of cumulus convection under a realistic constraint of a shortwave radiation timescale. By comparing the results of the present experiments and the previous studies on the diurnal variation of convective activity over the tropical ocean (Sui et al. 1997; Sui et al. 1998; Liu and Moncrieff 1998; Sato et al. 2009), this study will provide a clue to understanding the cumulus convection in the real atmosphere.

2. Numerical model and experimental setups

Numerical experiments are performed with the compressible, non-hydrostatic Weather Research and Forecasting (WRF) model (Skamarock et al. 2008) Ver.3.8.1. The following parameterizations are used: the WRF single–moment 6–class microphysics scheme (Hong and Lim 2006) that includes six classes of hydrometers (water vapor, cloud-water, rain, cloud-ice, snow, and graupel), the RRTMG shortwave/longwave schemes (Iacono et al. 2008) that use correlated-k method to calculate radiative fluxes and heating/cooling rates, the Monin-Obukhov surface scheme (Jimenez et al. 2012), and the first-order turbulence closure of the Smagorinsky model (Lilly 1962).

The shortwave radiation scheme includes a diurnal cycle which corresponds to the coordinate of zero degree latitude and longitude and starts at midnight of June 1st. Thus, Coriolis force is set to zero. Sea surface temperature (SST) is set to a constant, 301.5 K. A modification of bulk coefficients in the surface fluxes calculations, often done in RCE experiments (Wing and Emanuel 2014), was not implemented here. The domain size is vertically 25 km with Rayleigh damping in the upper 5-km layer, horizontally 200 km by 200 km (L200) with periodic lateral boundaries.

In order to examine dependencies on horizontal resolution and to ensure a trimodal vertical structure of tropical convection, we refer to Khairoutdinov et al. (2009) to set resolutions. There are 124 vertical levels, which stretch from about 50 m at the bottom, increasing to about 100 m at 4 km, about 500 m at 15 km, to about 2000 m at the top. The horizontal grid spacing was varied from 200 m (H200), 400 m (H400), 800 m (H800), to 1600 m (H1600).

The initial conditions of potential temperature and water vapor mixing ratio are specified based on the mean hurricane sounding for the West Indies area (Jordan 1958) and horizontal winds are specified to zero. All experiments are started with random potential temperature perturbation at the bottom of the domain and integrated for 20 days. To save time, experiment H200 is first run on a 100 km by 100 km area (L100) domain for 14 days, and periodic domain is unfolded to the area of L200 and the integration is continued for 6 days. Experiments H400, H800 and H1600 are run on L200 from the beginning to the end.

Corresponding author: Tomoro Yanase, Disaster Prevention Research Institute, Kyoto University, Gokasho, Uji, Kyoto 611-0011, Japan. E-mail: yanase_t@storm.dpri.kyoto-u.ac.jp.

3. Results

In all the experiments, deep convection exhibited nearly random spatial distribution and the atmosphere approached quasi-equilibrium states. Outgoing longwave radiation (OLR) and precipitable water (PW) after 20-day integration time are shown in Fig. 1. Figure 2 shows the temporal evolution of the domain-averaged OLR and PW. With the increase in the horizontal resolution, the OLR becomes generally smaller and the amplitude of diurnal variation becomes larger while the PW becomes higher and the amplitude of diurnal variation becomes larger.

As expected from the temporal variations of OLR and PW, each experiment except for H1600 exhibits a clear diurnal variation. The temporal variations of the domain-averaged total precipitation rate in the last 5 days are shown in Fig. 3. Except for H1600 (showing intermittent precipitation), all experiments exhibit diurnal variations characterized by stronger precipitation from night to predawn and weaker precipitation from noon to evening. Similar to OLR and PW, with a finer horizontal resolution, the amplitude of temporal variation of precipitation rate becomes larger.

To closely investigate the time variations of convective activities, the total mixing ratio of cloud water and cloud ice in the last 5 days is shown in Fig. 4. Each experiment except for H1600 exhibits a trimodal vertical structure, as reported in observations (Johnson et al. 1999; Takemi et al. 2004) and in high-resolution numerical simulations (Khairoutdinov et al. 2009). The diurnal variation represented in H1600 is only for low-topped clouds (cumulus; Cu) (Fig. 4d), while that in the other experiments is clearly seen for all the trimodal clouds (Figs. 4a, 4b, and 4c). In the daily mean over Day 20, a middle-topped cloud (congestus; Cg) tends to be enhanced and a cumulus tends to be relatively decreased with finer horizontal resolution (Fig. 5d).

Furthermore, the contributions of the precipitation by each trimodal cloud to the total precipitation rate and its temporal variation differ among the experiments. In Fig. 3, the temporal variations of the domain-averaged precipitation rates classified to each trimodal type (Cu, Cg, and cumulonimbus (Cb)) are also shown. Cu (Cg) precipitation is defined as surface precipitation falling from clouds whose tops are below the height of about 3000 (6100) m, as diagnosed by the total mixing ratio of rain, snow, and graupel being zero. Cb precipitation is classified as the residual. Table 1 summarizes the precipitation characteristics in Fig. 3. A domain-averaged precipitation rate (mm h^{-1}) (DP), a percentage contribution to the total precipitation rate (%) (CT), and the degree of precipitation intensity in rainy areas (mm h^{-1}) (PI), are averaged in the last 5 days. With the increase in the horizontal resolution, DP of the total and the Cb precipitation becomes smaller while DP of the Cg precipitation becomes larger. Similarly, with a finer resolution, CT of the Cb becomes smaller while CT of the Cg becomes larger. In addition, PI for Cg and Cb becomes smaller with the resolution increase.

We will next consider thermodynamics and dynamics of the clouds and their environmental conditions to investigate factors

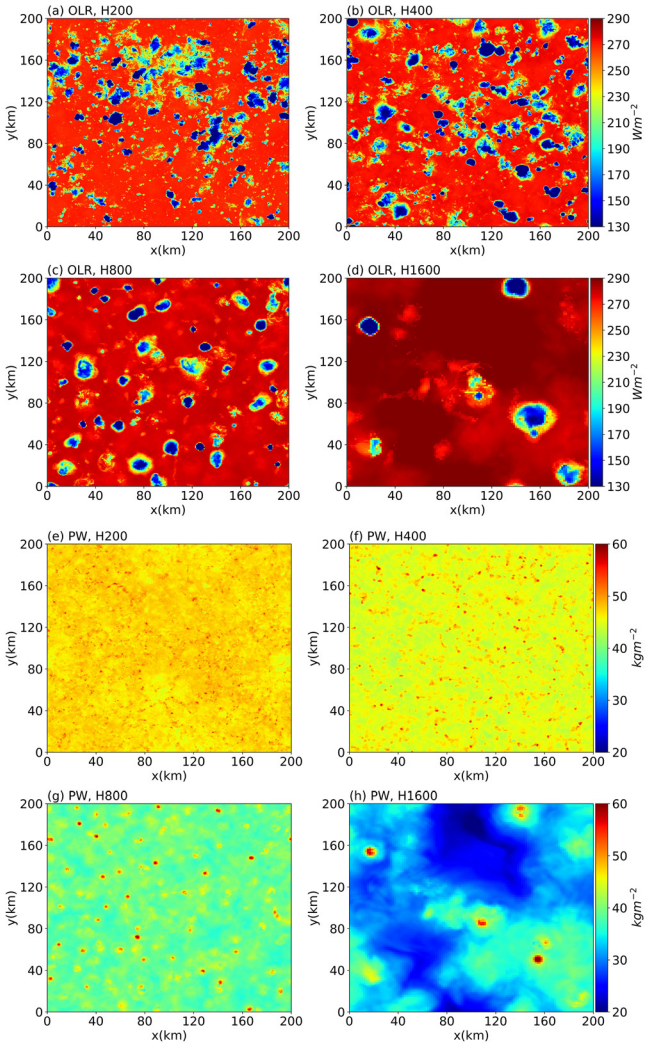

Fig. 1. Snapshots of outgoing longwave radiation (OLR) and precipitable water (PW) after integration over 20 days. OLR for (a) H200, (b) H400, (c) H800, and (d) H1600. PW for (e) H200, (f) H400, (g) H800, and (h) H1600.

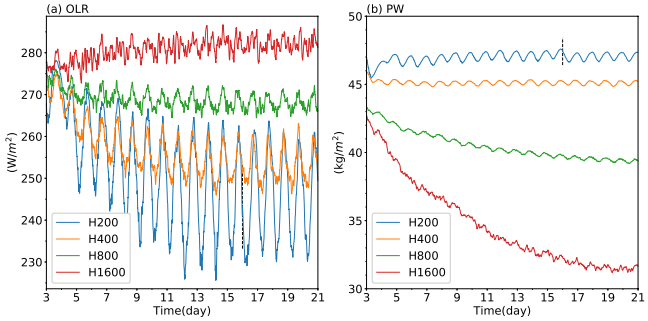

Fig. 2. Temporal evolution of domain-averaged (a) outgoing longwave radiation and (b) precipitable water from Day 3 to Day 20. The vertical dashed black lines indicate the time that H200 experiment switched from L100 to L200.

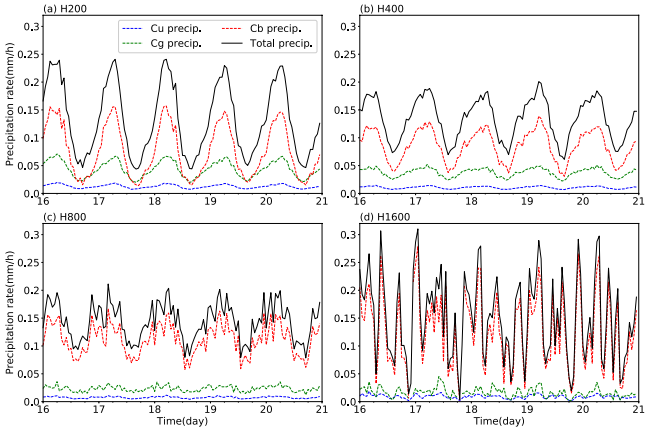

Fig. 3. Temporal evolution of domain-averaged precipitation rate on cumulus (blue dashed), congestus (green dashed), cumulonimbus (red dashed), and total (black solid) from Day 16 to Day 20 for (a) H200, (b) H400, (c) H800, and (d) H1600.

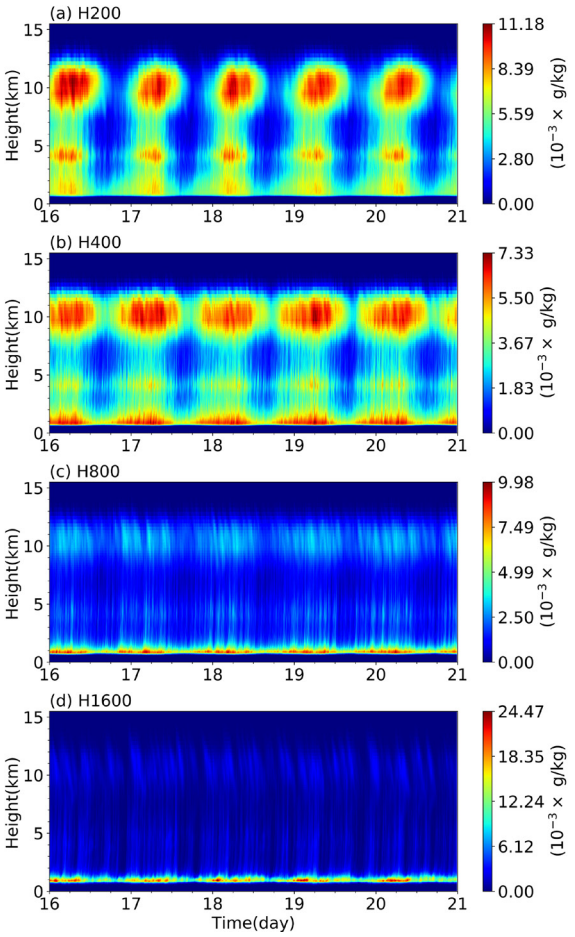

Fig. 4. Time-altitude cross sections of the horizontally-averaged total mixing ratio of cloud water and cloud ice from Day 16 to Day 20 for (a) H200, (b) H400, (c) H800, and (d) H1600. Color ranges are normalized to each maximum value.

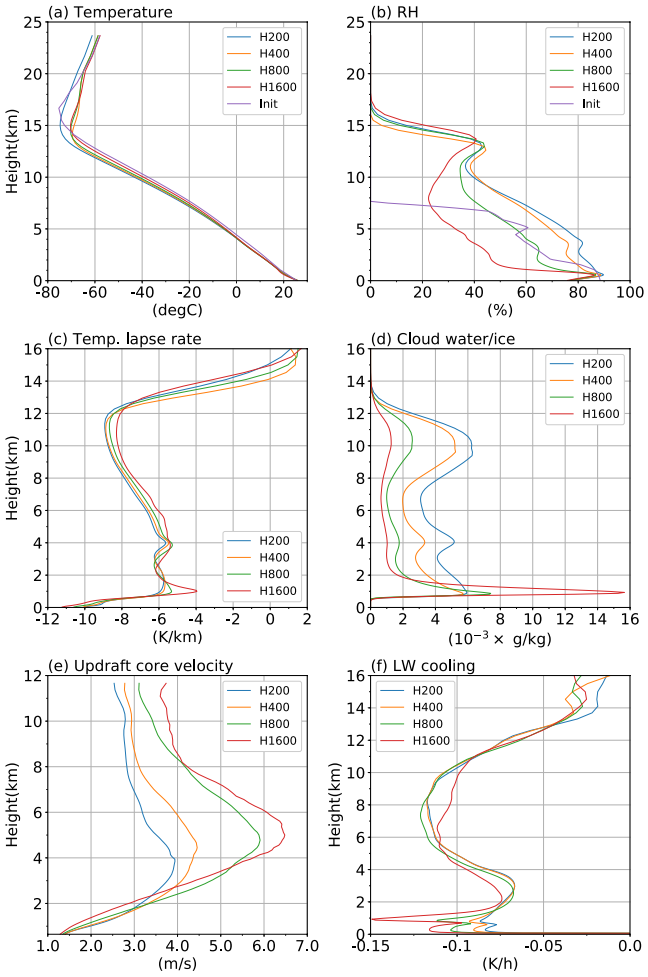

Fig. 5. Comparison of vertical profiles of daily mean horizontally-averaged (a) temperature, (b) relative humidity, (c) temperature lapse rate, (d) total mixing ratio of cloud water and ice, (e) updraft core velocity, and (f) longwave radiative cooling on Day 20. In (a) and (b), the initial states are also shown.

that make differences among the experiments in Fig. 5. The atmosphere appears to become more stable with the decrease in the horizontal resolution except for in the boundary layer, 2−4 km altitude, and above 10 km (Fig. 5a and 5c). As indicated by domain-averaged PW (Fig. 2b), the atmosphere becomes drier with coarser horizontal resolution, specifically in the layer of about 1−9 km height (Fig. 5b). Considering the trimodal feature of clouds (Fig. 5d), it is suggested that local maxima of RH near the middle troposphere (3−4 km) and the upper troposphere (12−14 km) correspond to Cg and Cb, respectively. The local maximum of RH in the middle troposphere appears most clearly in H200. The environment appears significantly drier in the coarser horizontal resolution than in Khairoutdinov et al. (2009). This is because they imposed the large-scale forcing such as tropospheric moistening, unlike the present study. Nevertheless, a larger amount of Cu is found with the decrease in the horizontal resolution in both the present experiments and Khairoutdinov et al. (2009). In addition, the large amount of Cu appears to contribute to a strong longwave cooling near the 1 km height (Fig. 5f). Next, to examine the dynamical features, we extracted updraft cores defined as grid points where the vertical velocity exceeds 1 m s^{-1} and the total mixing ratio of cloud-water/ice has a positive value. The updraft core velocity throughout the middle-to-upper troposphere becomes larger with the decrease in horizontal resolution while it is reversed in the lower troposphere (Fig. 5e). This updraft property is considered to explain why PI of the Cb precipitation is stronger with the coarser horizontal resolution (Table 1). However, the reason why the updrafts become stronger with the decrease in the horizontal resolution is not clear and will be discussed later.

Finally, we examine the mechanisms for the diurnal variation of cumulus convection by using the result of H200. According to past studies, the diurnal heat budget of the atmosphere is dominated by radiative heating cycle and net latent heating due to convection (Sui et al. 1998). It was also suggested that the difference of radiative heating between night and daytime affects the static stability of the troposphere (Liu and Moncrieff 1998). Thus, horizontally-averaged anomalies from the daily means of shortwave radiative heating, latent heating, and their sum are shown in Figs. 6a, 6b, and 6c. The anomaly of longwave radiative cooling is one order smaller than the others (not shown). Shown in Figs. 6d, 6e, and 6f are horizontally-averaged anomalies from the daily means of temperature, temperature lapse rate, and RH. Note that the negative (positive) anomaly of temperature lapse rate means destabilization (stabilization) of the atmosphere. While the phase of shortwave heating anomaly does not vary vertically, the amplitude varies (Fig. 6a). In the troposphere, the amplitude monotonically increases from the boundary layer to about 7-km height. Thus, the shortwave heating makes the lower-to-middle troposphere generally destabilized at night and stabilized in the daytime. On the other hand, both the phase and amplitude of latent heating anomaly vary vertically (Fig. 6b). Compared with Fig. 3a, when the precipitation rate is large (convection is active), the latent heating anomaly is positive above about 1 km and negative in the boundary layer. This negative anomaly is because of an enhanced evaporation of increased precipitation. The amplitude is

Table 1. Domain-averaged precipitation rate (DP) (mm h^{-1}), contribution to total precipitation (CT) (%), and a degree of precipitation intensity in rainy areas (PI) (mm h^{-1}) for each experiment and each trimodal type. They are averaged from Day 16 to Day 20.

	H200			H400			H800			H1600		
	DP	CT	PI	DP	CT	PI	DP	CT	PI	DP	CT	PI
Cu	0.013	9.6	0.186	0.011	7.9	0.185	0.008	5.3	0.161	0.009	6	0.198
Cg	0.044	32.8	1.404	0.038	28.2	1.937	0.023	16.3	2.245	0.016	10.7	2.913
Cb	0.076	57.6	1.699	0.086	63.9	2.561	0.112	78.4	5.228	0.125	83.3	11.239
Total	0.133	–	–	0.134	–	–	0.143	–	–	0.15	–	–

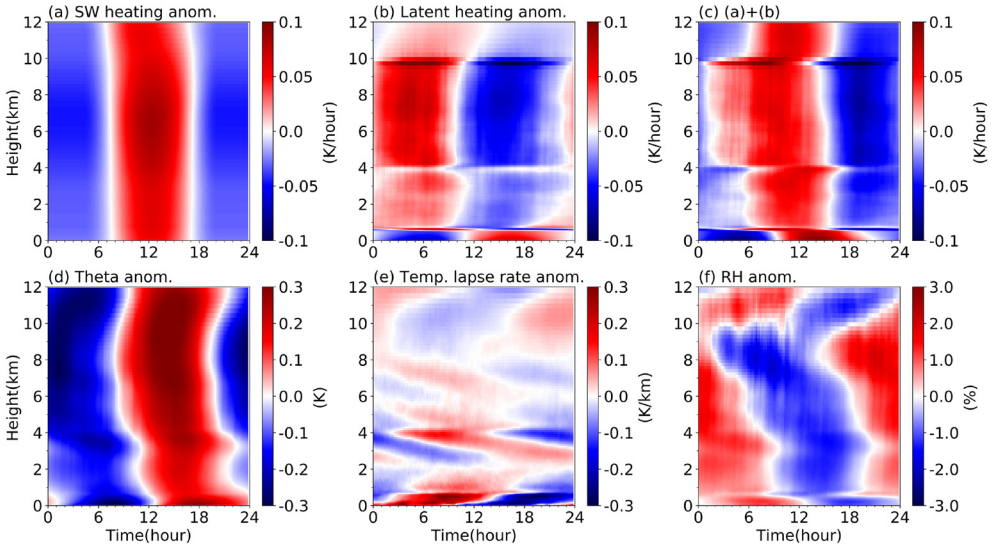

Fig. 6. Time-altitude cross-section of the horizontally-averaged anomalies from the daily mean of (a) shortwave radiative heating rate, (b) latent heating rate, (c) sum of (a)+(c), (d) potential temperature, (e) temperature lapse rate, and (f) relative humidity on Day 20. (a)–(c) are moving averaged in time for 4 hours.

notably suppressed in the lower-to-middle troposphere, especially at the melting layer about 4-km height. The sum of shortwave radiation and latent heating anomalies exhibit a distinct vertical feature (Fig. 6c). This affects the different temperature changes in the vertical, and the phase of the potential temperature anomaly inclines vertically (Fig. 6d). This inclination results in the temporal variation of temperature lapse rate anomaly with the phase shift in the vertical (Fig. 6e). Therefore, the daytime-nighttime contrast of the shortwave alone is insufficient to explain the variation of the stability of the atmosphere, and the effect of latent heating needs to be taken into account. This stability change suggests that more unstable (stable) atmosphere leads to stronger (weaker) precipitation in the nighttime (daytime). Furthermore, the RH anomaly appears to be inversely correlated with the potential temperature anomaly in the lower-to-middle troposphere (Fig. 6f). Assuming that positive (negative) anomaly of RH enhances (suppresses) the convective activities, the phase of RH anomaly is also consistent with the temporal variation of precipitation rate.

4. Discussion

While a convective organization like a single cluster is not seen in the experiments, spatial heterogeneity of PW, that is a signature of self-aggregation, appears in H1600 (Fig. 1). If domain size is sufficiently large, the spatial distribution of convection may change (Muller and Held 2012; Jeevanjee and Romps 2013). Nevertheless, the differences of OLR among the present experiments were comparable to those in self-aggregation experiments (Muller and Held 2012). This is because cloud and moisture largely affect longwave radiation in the atmosphere. As shown in Figs. 4 and 5, high-clouds are enhanced and low-clouds are suppressed with the increase in the horizontal resolution. Note that the large difference of longwave cooling among the experiments is mainly concentrated in the lower troposphere despite the large differences of humidity and clouds throughout the troposphere (Fig. 5).

The trimodal structure of clouds also affects the vertical distribution of RH that is tied to the convective updrafts. In the drier atmosphere, the buoyancy of convective cloud is not only enhanced by virtual temperature effect but also reduced by entrainment effect. As discussed by Wu et al. (2009), the transition from shallow to deep convection should be evaluated by the interaction of clouds and their environment. Also, the property of deep convection is known to vary in different cloud disturbances (Miyamoto et al. 2015) and the contribution of each cloud type to the total precipitation depends on the convective organization (Johnson et al. 1999). In the present experiments with coarser resolutions, a balance appears to exist between a larger precipitation rate due to Cb with strong updrafts and a larger water vapor flux from the sea surface by drier atmosphere. To understand how convection and its environment affect each other in RCE state, the present results should be compared to a various situation, for example, in which convection is organized at mesoscales.

Based on the above, here we discuss possible reasons why the diurnal variation appears less clearly with the decrease in the horizontal resolution and why there are still unknown issues in the mechanisms for the diurnal variation of cumulus convection. In order for the diurnal variation of surface precipitation to appear clearly, the transition process of cumulus to congestus or cumulonimbus should be simulated in response to a slight change in the environment field due to the diurnal variation of shortwave radiation. Such a response is produced not only by a mean environmental condition but also by convective-scale processes. For example, the entrainment process depends on the spatial scale of updrafts in the lower troposphere and the boundary layer. With the coarser horizontal resolution, it is suggested that the updrafts become less influenced by entrainment process under situations with the large amount of cumulus and intermittent vigorous cumulonimbus. Consequently, the diurnal variation becomes ambiguous with the decreased in the horizontal resolution. It is also suggested that the simulated RCE states highly depend on how turbulent structures are expressed in numerical models (Tompkins and Semie 2017).

Although this study suggested that convection is affected by the RH anomaly and the temperature lapse rate in the diurnal cycle, to what extent each anomaly is influential still needs to be quantitatively examined. To quantify them, the updraft core property in time and space should be investigated more closely. Specifically, the phase relationship among the diabatic forcings and the environmental conditions is consider to play a key role in determining diurnal variation of cumulus convection. By understanding how updrafts interact with their environments, we could understand why various types of clouds occur in nature and how cumulus convection exhibits diurnal variation.

Finally, as mentioned in the Radiative-Convective Equilibrium Model Intercomparison Project (Wing et al. 2018), a model configuration dependence should be systematically understood. Here, we conducted several high-resolution cloud-resolving RCE experiments over a relatively small domain with the diurnal variation of shortwave radiation and showed the dependencies of the diurnal variation of cumulus convection and trimodal vertical structure on horizontal resolution. The present dependence should be verified in various settings (e.g. larger domain size) because RCE is quite sensitive to model configurations. Nevertheless, it should be useful to verify the representation of tropical convection characteristics in order to tie the idealized RCE state and the real atmosphere, even in different model types.

5. Concluding remark

In order to understand tropical oceanic convection and its organization, past studies mostly focused on numerical experiments in radiative-convective equilibrium with constant shortwave forcing. In contrast, the present study examined how the diurnal variation of solar radiation affects the convective activity. We demonstrated, among the resolution cases examined, that the diurnal variation of cumulus convection is successfully reproduced by sub-kilometer horizontal resolution experiments while it is not represented by the 1600 m resolution experiment typically used in cloud-resolving simulations. It was also shown that the horizontal resolution dependence largely affects not only the representation of trimodal convection but also thermodynamic conditions and precipitation characteristics. Although the dependence of radiative-convective equilibrium state on model configuration has been previously recognized, we consider that there is a critical value of sub-kilometer horizontal resolution to represent the equilibrium state that consists of the interactions between convective scale process and its environment.

Acknowledgements

We thank the comments by two anonymous reviewers and Dr. Tomoe Nasuno to improve the original manuscript. This work was supported by JSPS Kakenhi 16H01846 and 18H01680 and the MEXT Post-K Project. The numerical experiments were conducted on the supercomputer of ACCMS, Kyoto University.

Edited by: T. Nasuno

References

Hong, S., and J. Lim, 2006: The WRF single-moment 6-class microphysics scheme (WSM6). *J. Korean Meteor. Soc.*, **42**, 129−151.

Iacono, M. J., J. S. Delamere, E. J. Mlawer, M. W. Shephard, S. A. Clough, and W. D. Collins, 2008: Radiative forcing by long-lived greenhouse gases: Calculations with the AER radiative transfer models. *J. Geophys. Res. Atmos.*, **113**, 2−9.

Jeevanjee, N., and D. M. Romps, 2013: Convective self-aggregation, cold pools, and domain size. *Geophys. Res. Lett.*, **40**, 994−998.

Jiménez, P. A., J. Dudhia, J. F. González-Rouco, J. Navarro, J. P. Montávez, and E. García-Bustamante, 2012: A revised scheme for the WRF surface layer formulation. *Mon. Wea. Rev.*, **140**, 898−918.

Johnson, R. H., T. M. Rickenbach, S. A. Rutledge, P. E. Ciesielski, and W. H. Schubert, 1999: Trimodal characteristics of tropical convection. *J. Climate*, **12**, 2397−2418.

Jordan, C. L., 1958: Mean soundings for the West Indies area. *J. Meteor.*, **15**, 91−97.

Khairoutdinov, M. F., S. K. Krueger, C.-H. Moeng, P. A. Bogenschutz, and D. A. Randall, 2009: Large-eddy simulation of maritime deep tropical convection. *J. Adv. Model. Earth Syst.*, **2**, 15.

Lilly, D. K., 1962: On the numerical simulation of buoyant convection. *Tellus*, **14**, 148−172.

Liu, C., and M. W. Moncrieff, 1998: A numerical study of the diurnal cycle of tropical oceanic convection. *J. Atmos. Sci.*, **55**, 2329−2344.

Miyamoto, Y., R. Yoshida, T. Yamaura, H. Yashiro, H. Tomita, and Y. Kajikawa, 2015: Does convection vary in different cloud disturbances? *Atmos. Sci. Lett.*, **16**, 305−309.

Muller, C. J., and I. M. Held, 2012: Detailed investigation of the self-aggregation of convection in cloud-resolving simulations. *J. Atmos. Sci.*, **69**, 2551−2565.

Nakajima, K., and T. Matsuno, 1988: Numerical experiments concerning the origin of cloud clusters in the tropical atmosphere. *J. Meteor. Soc. Japan. Ser. II*, **66**, 309−329.

Posselt, D. J., S. C. van den Heever, and G. L. Stephens, 2008: Trimodal cloudiness and tropical stable layers in simulations of radiative convective equilibrium. *Geophys. Res. Lett.*, **35**, 1−5.

Robe, F. R., and K. A. Emanuel, 2001: The effect of vertical wind shear on radiative–convective equilibrium states. *J. Atmos. Sci.*, **58**, 1427−1445.

Sato, T., H. Miura, M. Satoh, Y. N. Takayabu, and Y. Wang, 2009: Diurnal cycle of precipitation in the tropics simulated in a global cloud-resolving model. *J. Climate*, **22**, 4809−4826.

Skamarock, W. C., and co-authors, 2008: A description of the Advanced Research WRF Version 3. *Tech. Rep.*, 113.

Sui, C.-H., K.-M. Lau, Y. N. Takayabu, and D. A. Short, 1997: Diurnal variations in tropical oceanic cumulus convection during TOGA COARE. *J. Atmos. Sci.*, **54**, 639−655.

Sui, C.-H., X. Li, and K.-M. Lau, 1998: Radiative–convective processes in simulated diurnal variations of tropical oceanic convection. *J. Atmos. Sci.*, **55**, 2345−2357.

Takemi, T., O. Hirayama, and C. Liu, 2004: Factors responsible for the vertical development of tropical oceanic cumulus convection. *Geophys. Res. Lett.*, **31**, L11109, doi:10.1029/2004GL020225.

Tobin, I., S. Bony, and R. Roca, 2012: Observational evidence for relationships between the degree of aggregation of deep convection, water vapor, surface fluxes, and radiation. *J. Climate*, **25**, 6885−6904.

Tompkins, A. M., 2001: Organization of tropical convection in low vertical wind shears: The role of water vapor. *J. Atmos. Sci.*, **58**, 529−545.

Tompkins, A. M., and G. C. Craig, 1998: Radiative-convective equilibrium in a three-dimensional cloud-ensemble model. *Quart. J. Roy. Meteor. Soc.*, **124**, 2073−2097.

Tompkins, A. M., and A. G. Semie, 2017: Organization of tropical convection in low vertical wind shears: Role of updraft entrainment. *J. Adv. Model. Earth Syst.*, **9**, 1046−1068.

Wing, A. A., and K. A. Emanuel, 2013: Physical mechanisms controlling self-aggregation of convection in idealized numerical modeling simulations. *J. Adv. Model. Earth Syst.*, **6**, 59−74.

Wing, A. A., K. Emanuel, C. E. Holloway, and C. Muller, 2017: Convective self-aggregation in numerical simulations: A Review. *Surv. Geophys.*, 1−25.

Wing, A. A., K. A. Reed, M. Satoh, B. Stevens, S. Bony, and T. Ohno, 2018: Radiative-convective equilibrium model intercomparison project. *Geosci. Model Dev.*, **11**, 793−813.

Wu, C.-M., B. Stevens, and A. Arakawa, 2009: What controls the transition from shallow to deep convection? *J. Atmos. Sci.*, **66**, 1793−1806.

Yang, D., 2017: Boundary layer height and buoyancy determine the horizontal scale of convective self-aggregation. *J. Atmos. Sci.*, **75**, 469−478.

Yashiro, H., Y. Kajikawa, Y. Miyamoto, T. Yamaura, R. Yoshida, and H. Tomita, 2016: Resolution dependence of the diurnal cycle of precipitation simulated by a global cloud-system resolving model. *SOLA*, **12**, 272−276.

Manuscript received 18 April 2018, accepted 2 July 2018
SOLA: https://www.jstage.jst.go.jp/browse/sola/